Available online at www.sciencedirect.com
SCIENCE DIRECT®
Ocean Engineering 31 (2004) 455–482
OCEAN ENGINEERING
www.elsevier.com/locate/oceaneng

Nonlinear identification of mooring lines in dynamic operation of floating structures

Mario A. Jordán *, Reinel Beltrán-Aguedo

Dto. de Ingeniería Eléctrica, Universidad Nacional del Sur, Av. Alem 1253—(8000), Bahía Blanca, Argentina

Received 3 January 2003; received in revised form 3 June 2003; accepted 11 June 2003

Abstract

An adaptive algorithm for on-line estimation of physical coefficients of cables in viscous environment is presented. The procedure is useful for obtaining cable characteristics, which are needed in stability analysis and control system design for moored floating structures. It uses measurements of position and forces from on-board instrumentation. It is also able to track changes in the depth and to test for parameter consistency in order to confer the estimation robustness with respect to dynamic perturbations. It is based on nonlinear solvers, which can cope with transcendental functions of the model structure. The proof of asymptotic convergence is presented. Finally, three basic case studies are analyzed.

Keywords: Cable; Moored floating structure; Dynamic configuration; Static configuration; Adaptive algorithm; Nonlinear estimation; Algorithm convergence; Monochromatic excitation

1. Introduction

Cables are used extensively today in offshore industry and oceanographic community for stationing floating structures, and towing of underwater vehicles from a surface ship. The modelling of the cable response is very important for performing stability analysis of the over-all dynamics of a moored system (Kreuzer et al., 2002; Gottlieb and Yim, 1997; Dmitrieva and Lougovsky, 1997; Beltrán-Aguedo et al., 2002). Other important goal is the model-based regulation of the moored structure

* Corresponding author. Tel.: +54-291-4595100 x3310; fax: +54-291-4595154.
E-mail address: mjordan@criba.edu.ar (M.A. Jordán).

0029-8018/$ - see front matter
doi:10.1016/S0029-8018(03)00122-7

about a coordinate point despite disturbances of the environment (Aamo and Fossen, 1999; Sorensen et al., 1999).

An elastic cable submerged in a heavy fluid, such as water, combines soft transverse stiffness with a strong high-frequency axial stiffness (Mavrakos and Chatjigeorgiou, 1997; Mavrakos et al., 1996). In applications when the ratio of the elastic to the catenary stiffness is small and hydrodynamic drag loads are of low frequency, the mooring line preserves basically its catenary in-plane shape. In this case a quasi-static behavior takes place.

In stability analysis and control system design for moored floating systems, a range-dependent polynomial approximation of the cable characteristic is generally used. Herein a particular parameter set of the cable, constituted by mathematical coefficients, is investigated in order to explain a diversity of nonlinear behaviors (Gottlieb and Yim, 1997). On the other hand, using phenomenological equations of the catenary, it is possible to directly study the incidence of parameter changes, like initial tensions, mass and depth, maintaining a physical interpretation of the results.

Previous and related results are presented in Beltrán-Aguedo and Jordán (2003) for identifying mathematical parameters of the cable in moored semisubmersibles and in Gottlieb et al. (1996) for parameter estimation of mooring systems using Hilbert Transform. In Bhattacharyya and Selvam (2001), and Selvam and Bhattacharyya (2001), a procedure referred to as Reverse Multiple Inputs–Single Output method for identification of hydrodynamic coefficients as well as linear and nonlinear stiffness parameters of a cubic approximation of the mooring lines is presented. These last works include a simplified dynamics in a single degree of freedom with random excitation.

In the present paper, we provide a method for on-line identification of physical coefficients of a catenary from on-board-instrumentation measures related to regular operation of a moored system. The present approach requires only a few amount of knowledge of the mooring system configuration and of the cable itself. As hypothesis for the application it is demanded that only low till medium frequency components are present in the structure behavior, which is commonly accomplished by floating semisubmersibles. An additional property of the presented algorithm is that it can track time-varying parameters adaptively, like the sea depth.

2. Governing equations

In our physical configuration, the cable forms a catenary-like shape between an upper end attached to a floating structure and a point of the sea floor. The upper end of the cable is forced to follow an arbitrary motion including vertical and horizontal displacements, which are induced by the considered floating structure interacting with waves.

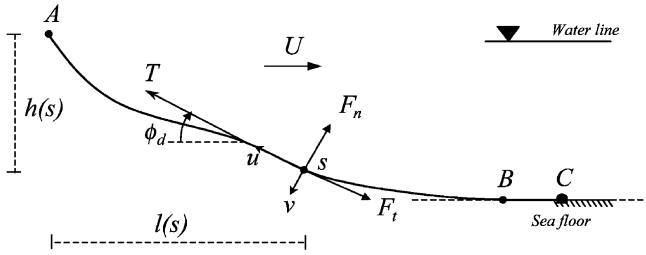

Fig. 1. Cable in dynamic configuration.

2.1. Dynamic configuration

The cable is conceived as a slender rod with negligible bending stiffness submersed in the sea (see Fig. 1). Let s denote the unstretched Lagrangian coordinate measured from the upper cable end up to some point of consideration on the cable, $\mathbf{v}(v_t, v_n)$ its velocity with tangential and normal components u and v, m_0 the mass per unit unstretched length (mass density), $\mathbf{T}$ the tangential tension vector, F the distributed drag force per unit stretched length and ε the local strain. Every material point s at the cable can be also referenced by horizontal and vertical coordinates, $l(s)$ and $h(s)$, respectively.

Then, the equations of motion of a cable having two-dimensional shape can be expressed along the local tangential, t, and normal, n, directions of its moving in-plane configuration as (Mavrakos and Chatjigeorgiou, 1997; Mavrakos et al., 1996; Papazoglou et al., 1996)

$$m_0\left(\frac{\partial u}{\partial t} - v\frac{\partial \phi_d}{\partial t}\right) = \frac{\partial \mathbf{T}}{\partial s} - w\sin(\phi_d) + F_t(1+\varepsilon) \tag{1}$$

$$m_0\left(\frac{\partial v}{\partial t} + u\frac{\partial \phi_d}{\partial t}\right) + m_a\frac{\partial v_r}{\partial t} = \mathbf{T}\frac{\partial \phi_d}{\partial s} - w\cos(\phi_d) + F_n(1+\varepsilon) \tag{2}$$

$$\frac{\partial \varepsilon}{\partial t} = \frac{\partial u}{\partial s} - v\frac{\partial \phi_d}{\partial s} \tag{3}$$

$$\frac{\partial \phi_d}{\partial t}(1+\varepsilon) = \frac{\partial v}{\partial s} + u\frac{\partial \phi_d}{\partial s}, \tag{4}$$

where m_a is the two-dimensional added mass per cable unit length, which is assumed to be equal to its potential-flow value for an infinitely long cylinder with the same cross-section, and w is the submerged weight per cable unit length. Moreover, ϕ_d is the angle formed by the horizontal and local tangential direction at the considered point s. This angle varies dynamically with the velocity $\mathbf{v}$ at any considered material point.

Additionally, the tension–strain relation is assumed to be linear according to the Hooke's law as

$$\mathbf{T} = EA\varepsilon\mathbf{t}, \tag{5}$$

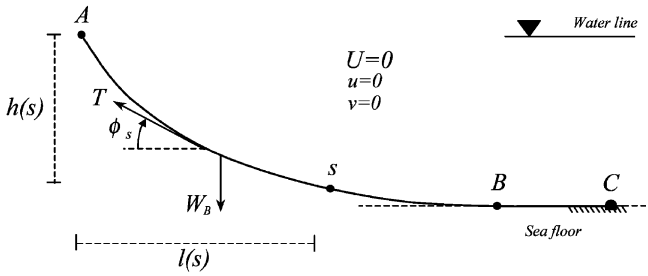

Fig. 2. Cable in static configuration.

with E the Young modulus and A the cross-section of the stretched cable. The drag forces are referred to the relative fluid-cable velocity as

$$F_t = 0.5\pi\rho_w c_f d(\mathbf{U}\cos\phi_d - u)|\mathbf{U}\cos\phi_d - u| \tag{6}$$

$$F_n = -0.5\pi\rho_w c_d d(\mathbf{U}\sin\phi_d + u)|\mathbf{U}\sin\phi_d + u|, \tag{7}$$

where ρ_w is the water density, c_f and c_d are the frictional and normal drag coefficients, respectively, d is the stretched cable diameter and $\mathbf{U}$ the local current velocity in the plane.

In the paper, we will suppose the solution of (1)–(4) to be the real evolution of the cable and thereby the one corresponding to the set of measurements to be apply for parameter estimation.

2.2. Static configuration

Let us meet following assumptions on the former dynamic configuration:

(a) drag forces are negligible, it is, $F_t = F_n = 0$.
(b) cable inertia forces and displaced fluid acceleration are zero, it is, $m_0(\partial u/\partial t) = m_0(\partial v/\partial t) = 0$, $m_a(\partial v_r/\partial t) = 0$.
(c) the motions of the cable and fluid are slow such that $u(\partial\phi_d/\partial t)$ and $v(\partial v/\partial t)$ are not meaningful.

Then, the partial differential Eqs. (1) and (2) get into the ordinary differential equations

$$\mathbf{T}\frac{dl}{dp} = H \tag{8}$$

$$\mathbf{T}\frac{dh}{dp} = V - W_B\frac{s}{L_B} \tag{9}$$

$$\left(\frac{dl}{dp}\right)^2 + \left(\frac{dh}{dp}\right)^2 = 1, \tag{10}$$

where p is the Lagrangian coordinate of the stretched profile under self-weight of the cable, H and V are the horizontal and vertical components of $\mathbf{T}$ at p, respect-

ively, with $\phi_s = \tan^{-1}(V/H)$. The variables W_B and L_B represent the weight of the cable lying over the sea floor and its unstretched length, respectively (see Fig. 2). The tension–strain relation is

$$\mathbf{T} = EA_0\left(\frac{\mathrm{d}p}{\mathrm{d}s} - 1\right)\mathbf{t}, \tag{11}$$

with A_0 the uniform cross-section in the unstretched cable.

The solution of (1)–(4) with (5)–(7) is performed numerically under some other plausible assumptions, which allow simplifications of the solution (Papazoglou et al., 1996; Chatjigeorgiou and Mavrakos, 2000). They show that the response of the cable is dominated by elastic stiffness (and not by catenary stiffness) for sufficiently high frequencies. A good approximation of the solution for the cable dynamics can however be obtained in the presence of low-frequency motions by solving (8)–(10) with (11). Herein, conditions (a)–(c) are supposed to be achieved approximately.

This way is important for a practical identification, because it requires sensors of forces at the upper end only. In contrast, using the structure (1)–(4), the identification would require the information of the distributed tension $\mathbf{T}(s)$ along the cable, which is difficult to implement with current force sensors.

The solution for the static configuration can be carried out analytically under the end conditions:

$$\begin{array}{ll} l = 0,\ h = 0,\ p = 0 & \text{at } s = 0 \\ l = l_B,\ h = h_B,\ p = L_B + \Delta L_B & \text{at } s = L_B, \end{array} \tag{12}$$

with l_B and h_B the horizontal and vertical coordinates of the contact point B, respectively, and ΔL_B the length variation calculated with (11) as

$$\Delta L_B = \int_0^{L_B} \frac{\mathrm{d}p}{\mathrm{d}s}\mathrm{d}s - L_B = \int_0^{L_B}\left(\frac{\sqrt{H^2(s) + V^2(s)}}{EA_0} + 1\right)\mathrm{d}s - L_B. \tag{13}$$

The solution of (8)–(10) is (cf. Irvine, 1992)

$$\mathbf{T}(s) = \begin{cases} \sqrt{H^2 + \left(V - W_B\dfrac{s}{L_B}\right)^2}\,\mathbf{t} & \text{for } 0 \le s \le L_B \\ H\mathbf{t} & \text{for } L_B < s \le L_0 \end{cases} \tag{14}$$

$$l(s) = \begin{cases} \dfrac{Hs}{EA_0} + \dfrac{HL_B}{W_B}\left(\sinh^{-1}\left(\dfrac{V}{H}\right) - \sinh^{-1}\left(\dfrac{V - W_B s/L_B}{H}\right)\right) \\ \quad \text{for } 0 \le s \le L_B \\ l(L_B) + s - L_B \\ \quad \text{for } L_B < s \le L_0 \end{cases} \tag{15}$$

$$h(s)=\begin{cases}\dfrac{W_B L_B}{EA_0}\left(\dfrac{V}{W_B}-\dfrac{s}{2L_B}\right)+\dfrac{HL_B}{W_B}\left(\sqrt{1+\left(\dfrac{V}{H}\right)^2}-\sqrt{1+\left(\dfrac{V-W_B s/L_B}{H}\right)^2}\right)\\ \quad \text{for } 0\le s\le L_B\\ h(L_B)\\ \quad \text{for } L_B< s\le L_0\end{cases} \tag{16}$$

with $l(L_B)=l_B$, $h(L_B)=h_B$ and L_0 the total unstretched length from A to C.

3. Identification

From the point of view of the identification we are interested in the on-line estimation of physical coefficients of a cable attached to a floating structure in operation. So we start from a static model yet with real measurements, i.e. position and forces of the dynamic configuration.

The presented algorithm performs two basic tasks on-line. The first task comprehends an adaptive parameter estimation using the model structure of the static configuration. The second task includes a filtering of the estimates for minimizing the energy of the parameter errors, which appear due to the dynamic measurements.

3.1. Setup for measurements

Our start point is the measure of the signal set

$$\{x(t),\ z(t),\ V(t),\ H(t)\} \tag{17}$$

in continuous time t, where

$$x(t)=l_0-l(t) \tag{18}$$

$$z(t)=h_0-h(t), \tag{19}$$

describe the position trajectory, with $(l_0,\ h_0)$ and $(l(t),\ h(t))$ being lengths corresponding to the horizontal and vertical coordinates of A in static equilibrium and in arbitrary position of the stretched cable, respectively. The forces H and V are the components of $\mathbf{T}$ at A (Fig. 3).

The set of physical coefficients to be identified is

$$\{m_0,\ EA_0,\ l_0,\ h_0\}. \tag{20}$$

One serious problem for the development of an algorithm for identification constitutes the fact that the angle ϕ_s at the contact point B produces a structural change of the mathematical structure in Eqs. (14)–(16) when its value transits from zero to a positive angle and vice versa. This problem is evidenced in the next.

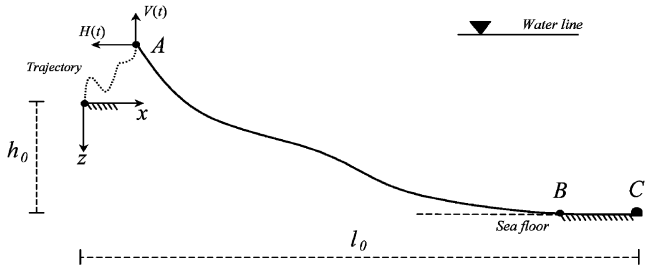

Fig. 3. Cable configuration with measured signals.

3.2. Geometrical shapes

The angle-depending solution of the catenary equations involves two particular geometrical shapes in the static configuration. These are referred to throughout the paper as Case I and II.

Case I. $\phi_s > 0$ This case concerns the superposition of points B and C with an angle $\phi_s > 0$. Using

$$\max L_B = L_0 \tag{21}$$

$$\max W_B = W_0 = m_0 g L_0, \tag{22}$$

the solution (15) and (16) turns particularly into

$$l(L_0) = \frac{HL_0}{EA_0} + \frac{H}{m_0 g}\left(\sinh^{-1}\left(\frac{V}{H}\right) - \sinh^{-1}\left(\frac{V - m_0 g L_0}{H}\right)\right) \tag{23}$$

$$h(L_0) = \frac{m_0 g L_0}{EA_0}\left(\frac{V}{m_0 g} - \frac{L_0}{2}\right) + \frac{H}{m_0 g} \times \left(\sqrt{1 + \left(\frac{V}{H}\right)^2} - \sqrt{1 + \left(\frac{V - m_0 g L_0}{H}\right)^2}\right), \tag{24}$$

where the vertical force component results

$$V = m_0 g L_0 + R, \tag{25}$$

with R the vertical reaction at the anchored point C.

Case II. $\phi_s = 0$ The second case describes a set of catenary shapes with the property $\phi_s = 0$ at B. The solution is characterized by V that is only due to the self-

weight W_B. Consequently, (15) and (16) become

$$l(L_0) = \frac{HL_B}{EA_0} + \frac{H}{m_0 g}\sinh^{-1}\left(\frac{V}{H}\right) + L_0 - L_B \tag{26}$$

$$h(L_0) = \frac{VL_B}{2EA_0} + \frac{H}{m_0 g}\left(\sqrt{1+\left(\frac{V}{H}\right)^2} - 1\right), \tag{27}$$

with

$$V = W_B = m_0 g L_B \tag{28}$$

$$R = 0. \tag{29}$$

It is clear that the equation sets (23) and (24) and (26) and (27) are structurally different, however they show continuity for B coinciding with C and $\phi_s = 0$. Moreover, in Case II appears a new nonmensurable state L_B, which contrasts with the Case I where this variable becomes constant in H and V and equal to L_0.

In quasi-static operation, the catenary shape may turn from one case into the other one. For the identification it is important to recognize the real case in order to apply the right set of equations.

The observability of one case from data (17) is not a trivial task. For instance, if the derivative in time of L_B is invoked indirectly to this goal, with (25) and (28) and (29)

$$m_0 g \frac{\mathrm{d}L_B}{\mathrm{d}t} = \frac{\mathrm{d}}{\mathrm{d}t}(V - R), \tag{30}$$

then

$$\frac{\mathrm{d}}{\mathrm{d}t}(V - R) > 0 \Rightarrow \text{case I} \tag{31}$$

$$\frac{\mathrm{d}}{\mathrm{d}t}(V - R) = 0 \Rightarrow \text{case II}. \tag{32}$$

But this method implies the measure of the reaction R, which is not in our data set. On the other hand, the measure of R requires a sensor on cable end at the sea bottom, which is unusual. A proposed way to the solution is described in the next.

3.3. Observability of Cases I and II

In order to establish the detectability of each case upon data, let us first combine (18) and (19) with (26) and (27) in the Case II with $l(t) = l(L_0)$ and $h(t) = h(L_0)$,

so as to obtain two independent expressions for the mass density m_0, it is

$$m_{0_x} = \frac{1}{l_0 - L_0 - x}\left(\frac{HV}{EA_0 g} + \frac{H}{g}\sinh^{-1}\left(\frac{V}{H}\right) - \frac{V}{g}\right) \tag{33}$$

$$m_{0_z} = \frac{1}{h_0 - z}\left(\frac{V^2}{2EA_0 g} + \frac{H}{g}\left(\sqrt{1 + \left(\frac{V}{H}\right)^2} - 1\right)\right), \tag{34}$$

where m_{0_x} and m_{0_z} are the mass densities evaluated independently by measurements of x and z, respectively.

In real operations, the approximations: $EA_0 g \gg \max(HV), L_0 - l_0 \gg |x(t)|$ and $h_0 \gg |z(t)|$ are quite valid for all t. Taking these into account and equaling (33) and (34) one gets

$$\frac{h_0}{l_0 - L_0}\left(\sin\ \mathrm{h}^{-1}\left(\frac{V}{H}\right) - \frac{V}{H}\right) - \sqrt{1 + \left(\frac{V}{H}\right)^2} + 1 = 0, \tag{35}$$

which describes the linear locus in the plane H–V

$$V = cH, \tag{36}$$

with c a constant obtained implicitly from

$$\frac{\sqrt{(1 + c^2)} - 1}{\sinh^{-1}(c) - c} = \frac{h_0}{l_0 - L_0}. \tag{37}$$

Analogously, for the Case I, we can establish a similar relation for the set (23) and (24) under the same practical approximations like those assumed above.

Equivalently, the locus for the Case I results from (18) and (19) with (23) and (24) with $m_{0_x} g L_0 = m_{0_z} g L_0 = W_0$

$$\frac{h_0}{l_0 - L_0}\sinh^{-1}\left(\frac{V}{H}\right) - \sqrt{1 + \left(\frac{V}{H}\right)^2} = \frac{h_0}{l_0 - L_0}\sinh^{-1}\left(\frac{V - W_0}{H}\right) - \sqrt{1 + \left(\frac{V - W_0}{H}\right)^2}, \tag{38}$$

which can be solved analytically for H and V for $V > W_0$ achieving the expression

$$V = aH + b, \tag{39}$$

with a being obtained implicitly from

$$\frac{h_0}{l_0 - L_0}\sinh^{-1}\left(a + \frac{((c - a)/c)W_0}{H_1}\right) - \sqrt{1 + \left(a + \frac{((c - a)/c)W_0}{H_1}\right)^2} - \frac{h_0}{l_0 - L_0}\sinh^{-1}\left(a - \frac{(a/c)W_0}{H_1}\right) + \sqrt{1 + \left(a - \frac{(a/c)W_0}{H_1}\right)^2} = 0 \tag{40}$$

and b directly from

$$b = W_0 \frac{c-a}{c}, \tag{41}$$

where H_1 is some value greater than W_0/c.

The loci (36) and (39) in the space H–V are depicted in Fig. 4 for different ratios h_0/l_0.

It is noticed that the linear loci $m_{0_x} - m_{0_z} = 0$ for the Cases I and II are continuously connected with a break point at $(W_0/c,\ W_0)$. Moreover, a metric between two loci with different ratios h_0/l_0 is the larger the smaller these ratios h_0/l_0.

The main conclusion of this analysis is threefold. First, given a set of static forces (H, V), only one case can reproduce equality of mass densities, i.e. $m_{0_x} = m_{0_z}$, while simultaneously the other set of equations gives $m_{0_x} \neq m_{0_z}$. Secondly, the detectability of a case with respect to eventual perturbations in the static forces becomes high in the vicinity of $(W_0/c,\ W_0)$. Finally, if some degree of uncertainty is assumed in the parameters h_0 and l_0, then the disagreements $m_{0_x} \neq m_{0_z}$ of the equalities in Cases I and II, respectively, with respect to a mismatch in the ratio h_0/l_0 is the smaller the smaller is this ratio. This is also seen from the sensitivity function $\partial(m_{0_x} - m_{0_z})/\partial h_0$, which remains constant with respect to the depth h_0, and from the sensitivity function $\partial(m_{0_x} - m_{0_z})/\partial l_0$, which decreases proportional to l_0^2.

In summarize, the case observability is technically possible by this way. More details are given in Section 4.1.

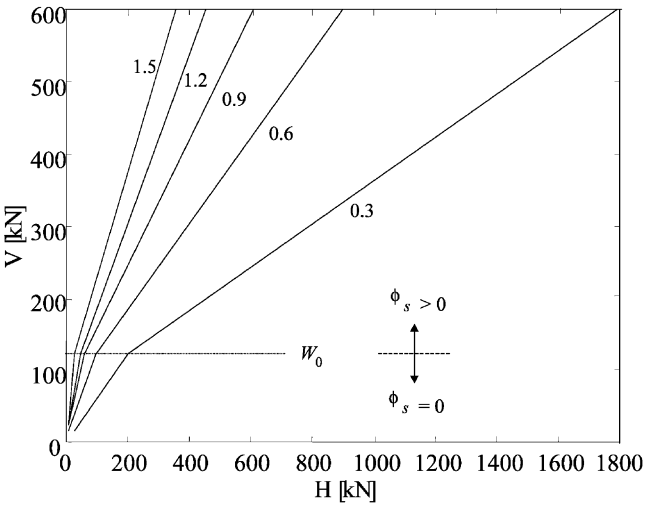

Fig. 4. Loci $m_{0_x} - m_{0_z} = 0$ in the plane H–V, parameterized in h_0/l_0 in the Cases I and II for $h_0 = 100$ [m] and $L_0 = 540$ [m].

3.4. Estimation in the static configuration

The Eqs. (15) and (16) are taken as support for the estimation. However, it is noticed that the number of parameters in (20) is greater than the only two available equations. Hence, parameter identifiability cannot be achieved by this way.

Another possibility is to create additional manifolds. To this end, let us define the solution of the estimation problem in the following manner. First consider manifolds of the form

$$f_{x_j}\left(U_{t_j}, f_c; \boldsymbol{\theta}_x\right) = 0 \tag{42}$$

$$f_{z_j}\left(U_{t_j}, f_c; \boldsymbol{\theta}_z\right) = 0 \tag{43}$$

with

$$U_{t_j} = \left\{x(t_j), z(t_j), H(t_j), V(t_j)\right\}, \text{ for } t_j \subseteq [t-T, t], \text{ and } j = 1, \ldots, n; \quad T > 0, \tag{44}$$

$$f_c = \begin{cases} 1 & \text{for case I} \\ 0 & \text{for case II} \end{cases}, \tag{45}$$

where the parameter vectors $\boldsymbol{\theta}_x$ and $\boldsymbol{\theta}_z$ contain the unknown system coefficients (20), U_{t_j} is a measurement set according (17), f_c is a case-sensitive function, t_j are sample time points, and n describes the number of the necessary data sets.

Moreover, $n_1 = \dim(\boldsymbol{\theta}_x)$ and $n_2 = \dim(\boldsymbol{\theta}_z)$, then

$$n = \frac{n_1 + n_2}{2}. \tag{46}$$

Thus, by defining conveniently $f_{x_j} = 0$ and $f_{z_j} = 0$ together with a proper selection of the t_i's, the intended estimation results technically viable.

Generically, the solution of the estimation problem consists hereafter in solving the system of $(n_1 + n_2)$ Eqs. (42) and (43) iteratively upon n data sets (44) in order to find $\boldsymbol{\theta}_x$ and $\boldsymbol{\theta}_z$.

3.5. Manifolds for estimation

With $s = L_0$ and $L_B = W_B/m_0 g$ in (15) and (16) we can establish the manifolds

$$f_{x_j} = x - (l_0 - (1-f_c)L_0) + f_c\frac{L_0 H}{EA_0} + (1-f_c)\frac{HV}{EA_0 m_0 g} + \frac{1}{m_0 g}\left(H\sinh^{-1}\left(\frac{V}{H}\right) - f_c H\sinh^{-1}\left(\frac{V - L_0 m_0 g}{H}\right) - (1-f_c)V\right) = 0 \tag{47}$$

$$f_{z_j} = z - \left(h_0 + f_c\frac{L_0^2 m_0 g}{2EA_0}\right) + f_c\frac{L_0 V}{EA_0} + (1-f_c)\frac{V^2}{2EA_0 m_0 g} + \frac{H}{m_0 g}\left(\sqrt{1+\left(\frac{V}{H}\right)^2} - \sqrt{1+f_c\left(\frac{V - L_0 m_0 g}{H}\right)^2}\right) = 0. \tag{48}$$

A glance at the structure of Eqs. (47) and (48) reveals that m_0 relays in a non-algebraic form as argument in transcendental functions. Moreover, there exist multilinearities between EA_0 and m_0, which hinder a direct identifiability of them.

In order to make the estimation of the physical coefficients (20) possible, we redefine the coefficients to be estimated in (47) and (48) as

$$x + a_1 + a_2 f_c H + a_3(1-f_c)HV + a_4\left(H\sinh^{-1}\left(\frac{V}{H}\right) - f_c H\sinh^{-1}\left(\frac{V - L_0/a_4}{H}\right) - 1(1-f_c)V\right) = 0 \tag{49}$$

$$z + b_1 + b_2 f_c V + b_3 V^2(1-f_c) + b_4 H\left(\sqrt{1+\left(\frac{V}{H}\right)^2} - \sqrt{1+f_c\left(\frac{V - L_0/b_4}{H}\right)^2}\right) = 0, \tag{50}$$

where the estimates are arrayed in the parameter vectors

$$\boldsymbol{\theta}_x = \begin{cases} [a_1, a_2, a_4]^{\mathrm{T}} & \text{for case I} \\ [a_1, a_3, a_4]^{\mathrm{T}} & \text{for case II} \end{cases} \tag{51}$$

$$\boldsymbol{\theta}_z = \begin{cases} [b_1, b_2, b_4]^{\mathrm{T}} & \text{for case I} \\ [b_1, b_3, b_4]^{\mathrm{T}} & \text{for case II} \end{cases} \tag{52}$$

for f_{x_j} and f_{z_j}, respectively. Consequently, according to (46), $n = n_1 = n_2 = 3$.

The identifiability of the physical coefficients is assured by

$$m_0 = \begin{cases} \dfrac{1}{a_4 g}; \\ \dfrac{1}{b_4 g} \end{cases} \qquad EA_0 = \begin{cases} L_0/a_2, & \text{for } f_c = 1 \\ L_0/b_2, & \\ \dfrac{a_4}{a_3}, & \text{for } f_c = 0 \\ \dfrac{b_4}{2b_3} & \end{cases}$$
$$l_0 = -a_1 + (1-f_c)L_0; \tag{53}$$
$$h_0 = -b_1 - f_c\frac{L_0}{2}\frac{b_2}{b_4};$$

It is noticed in (53) the optional forms to estimate m_0 and EA_0. Typical values for EA_0 are generally in an order of magnitude many times larger than those for the other parameters. Unless forces are relatively very large, a_2, a_3, b_2 and b_3 are difficult to estimate, specially a_2 and b_2 for the Case II.

4. Nonlinear estimation algorithm

The start point for designing an estimator are the definitions of f_{x_j} and f_{z_j} in (49) and (50). To this goal, consider

$$\begin{bmatrix} f_{x_1}(U_{t_1}, f_c; \boldsymbol{\theta}_x) \\ \vdots \\ f_{x_3}(U_{t_3}, f_c; \boldsymbol{\theta}_x) \end{bmatrix} = \mathbf{f}_x(U_t, f_c; \boldsymbol{\theta}_x) = 0 \tag{54}$$

$$\begin{bmatrix} f_{z_1}(U_{t_1}, f_c; \boldsymbol{\theta}_z) \\ \vdots \\ f_{z_3}(U_{t_3}, f_c; \boldsymbol{\theta}_z) \end{bmatrix} = \mathbf{f}_z(U_t, f_c; \boldsymbol{\theta}_z) = 0, \tag{55}$$

where $t_3 < t_2 < t_1 = t \subseteq [t-T, t)$, $U_t = U_{t_1} \cup U_{t_2} \cup U_{t_3}$ and f_c indicates a common case for the t_j's.

Due to the nonalgebraicity of (49) and (50), the proposed algorithm have to be designed in such a way that the solution results iteratively. Let the symbol $(\hat{\cdot})$ indicate an estimated variable. Then $\mathbf{f}_x\left(U_t, f_c; \hat{\boldsymbol{\theta}}_x\right)$ and $\mathbf{f}_z\left(U_t, f_c; \hat{\boldsymbol{\theta}}_z\right)$ are generally unequal to zero.

Now let us define

$$\begin{bmatrix} \mathbf{f}_x\left(U_t, f_c; \hat{\boldsymbol{\theta}}_x\right) \\ \mathbf{f}_z\left(U_t, f_c; \hat{\boldsymbol{\theta}}_z\right) \end{bmatrix} \stackrel{\text{def}}{=} \begin{bmatrix} \mathbf{g}_x\left(U_t, f_c; \hat{\boldsymbol{\theta}}_x\right) \\ \mathbf{g}_z\left(U_t, f_c; \hat{\boldsymbol{\theta}}_z\right) \end{bmatrix} - \begin{bmatrix} \mathbf{h}_x\left(U_t, f_c; \hat{\boldsymbol{\theta}}_x\right) \\ \mathbf{h}_z\left(U_t, f_c; \hat{\boldsymbol{\theta}}_z\right) \end{bmatrix}, \tag{56}$$

with a particular selection of g_x, g_z, h_x and h_z as

$$\begin{bmatrix} \mathbf{g}_x\left(U_t, f_c; \hat{\boldsymbol{\theta}}_x\right) \\ \mathbf{g}_z\left(U_t, f_c; \hat{\boldsymbol{\theta}}_x\right) \end{bmatrix} \stackrel{\text{def}}{=} \begin{bmatrix} \hat{\boldsymbol{\theta}}_x \\ \hat{\boldsymbol{\theta}}_z \end{bmatrix} \tag{57}$$

$$\begin{bmatrix} \mathbf{h}_x\left(U_t, f_c; \hat{\boldsymbol{\theta}}_x\right) \\ \mathbf{h}_z\left(U_t, f_c; \hat{\boldsymbol{\theta}}_z\right) \end{bmatrix} \stackrel{\text{def}}{=} \begin{bmatrix} \hat{\boldsymbol{\theta}}_x \\ \hat{\boldsymbol{\theta}}_z \end{bmatrix} - \mathbf{K}_t^{-1} \begin{bmatrix} \mathbf{f}_x\left(U_t, f_c; \hat{\boldsymbol{\theta}}_x\right) \\ \mathbf{f}_z\left(U_t, f_c; \hat{\boldsymbol{\theta}}_z\right) \end{bmatrix}. \tag{58}$$

Then, for an initial vector $\left[\hat{\boldsymbol{\theta}}_x^{(0)\mathrm{T}}, \hat{\boldsymbol{\theta}}_z^{(0)\mathrm{T}}\right]^{\mathrm{T}}$ the following series is generated

$$\begin{bmatrix} \hat{\boldsymbol{\theta}}_x^{(m)} \\ \hat{\boldsymbol{\theta}}_z^{(m)} \end{bmatrix} = \begin{bmatrix} \hat{\boldsymbol{\theta}}_x^{(m-1)} \\ \hat{\boldsymbol{\theta}}_z^{(m-1)} \end{bmatrix} - \mathbf{K}_t^{-1} \begin{bmatrix} \mathbf{f}_x\left(U_t, f_c; \hat{\boldsymbol{\theta}}_x^{(m-1)}\right) \\ \mathbf{f}_z\left(U_t, f_c; \hat{\boldsymbol{\theta}}_z^{(m-1)}\right) \end{bmatrix} \tag{59}$$

with the Jacobian

$$\mathbf{K}_t = \begin{bmatrix} \left.\dfrac{\partial \mathbf{f}_x^{\mathrm{T}}}{\partial \hat{\boldsymbol{\theta}}_x}\right|_{(U_t, f_c; \hat{\boldsymbol{\theta}}_x^{(m-1)})} & 0 \\ 0 & \left.\dfrac{\partial \mathbf{f}_z^{\mathrm{T}}}{\partial \hat{\boldsymbol{\theta}}_z}\right|_{(U_t, f_c; \hat{\boldsymbol{\theta}}_z^{(m-1)})} \end{bmatrix} \tag{60}$$

and elements $k_{ij} = \partial f_{x_j}\left(U_{t_j}, f_c; \hat{\boldsymbol{\theta}}_x\right)/\partial\hat{\theta}_{x_i}$ for the upper diagonal submatrix, and $k_{ij} = \partial f_{z_j}\left(U_{t_j}, f_c; \hat{\boldsymbol{\theta}}_z\right)/\partial\hat{\theta}_{z_i}$ for the lower diagonal submatrix, where $\hat{\theta}_{x_i}$ and $\hat{\theta}_{z_i}$ are elements of $\hat{\boldsymbol{\theta}}_x$ and $\hat{\boldsymbol{\theta}}_z$, respectively. More precisely

$$
\begin{aligned}
&\partial f_{x_j}\left(U_{t_j}, f_c; \hat{\boldsymbol{\theta}}_x\right)\Big/\partial\hat{a}_1 = 1\\
&\partial f_{x_j}\left(U_{t_j}, 1; \hat{\boldsymbol{\theta}}_x\right)\Big/\partial\hat{a}_2 = H_j\\
&\partial f_{x_j}\left(U_{t_j}, 0; \hat{\boldsymbol{\theta}}_x\right)\Big/\partial\hat{a}_3 = H_j V_j\\
&\partial f_{x_j}\left(U_{t_j}, f_c; \hat{\boldsymbol{\theta}}_x\right)\Big/\partial\hat{a}_4 = -(1-f_c)V - \frac{f_c L_0/\hat{a}_4}{\sqrt{1+\left(\dfrac{V_j - L_0/\hat{a}_4}{H_j}\right)^2}}\\
&+H_j\left(\sinh^{-1}\left(\frac{V_j}{H_j}\right) - f_c\sinh^{-1}\left(\frac{V_j - L_0/\hat{a}_4}{H_j}\right)\right)\\
&\partial f_{z_j}\left(U_{t_j}, f_c; \hat{\boldsymbol{\theta}}_x\right)\Big/\partial\hat{b}_1 = 1\\
&\partial f_{z_j}\left(U_{t_j}, 1; \hat{\boldsymbol{\theta}}_x\right)\Big/\partial\hat{b}_2 = V_j\\
&\partial f_{z_j}\left(U_{t_j}, 0; \hat{\boldsymbol{\theta}}_x\right)\Big/\partial\hat{b}_3 = V_j^2\\
&\partial f_{z_j}\left(U_{t_j}, f_c; \hat{\boldsymbol{\theta}}_x\right)\Big/\partial\hat{b}_4 = -\frac{f_c L_0\left(V_j - L_0/\hat{b}_4\right)}{\hat{b}_4 H\sqrt{1+f_c\left(\dfrac{V_j - L_0/\hat{b}_4}{H_j}\right)^2}}\\
&+H_j\left(\sqrt{1+\left(\frac{V_j}{H_j}\right)^2} - \sqrt{1+f_c\left(\frac{V_j - L_0/\hat{b}_4}{H_j}\right)^2}\right),
\end{aligned}
\tag{61}
$$

with $H_j = H(t_j)$ and $V_j = V(t_j)$.

4.1. The case-sensitive function f_c

As seen in (53) there are multiple ways to estimate m_0 and EA_0. They may be used properly for the detectability of Cases I and II, i.e. by implementing matching equations $m_{0_x} = m_{0_z}$ or $EA_{0_x} = EA_{0_z}$. However, it is remarkable that the parameter EA_0 is generally difficult to estimate unless the forces are very large. From these reason, the more proper way to detect case is through m_0.

To implement f_c we formulate a hypothesis that requires the estimation of $\boldsymbol{\theta}_x$ and $\boldsymbol{\theta}_z$ for both cases independently. Accordingly, we define $f_c = 1$ and verify if for some small positive real number ε, the inequality

$$
\left|\hat{a}_4 - \hat{b}_4\right| \le \varepsilon \text{ for} \begin{cases} \mathbf{f}_x(U_t, 1; \boldsymbol{\theta}_x) = 0 \\ \mathbf{f}_z(U_t, 1; \boldsymbol{\theta}_z) = 0 \end{cases} \tag{62}
$$

is satisfied, where $\hat{a}_4$ and $\hat{b}_4$ are related to m_{0_x} and m_{0_z}, respectively, by the expressions given in (53). If not, we change the hypothesis $f_c = 0$ and test the next inequality

$$\left|\hat{a}_4 - \hat{b}_4\right| \leq \varepsilon \text{ for} \begin{cases} \mathbf{f}_x(U_t, 0; \boldsymbol{\theta}_x) = 0 \\ \mathbf{f}_z(U_t, 0; \boldsymbol{\theta}_z) = 0 \end{cases}. \tag{63}$$

If the data are not perturbed, one of the hypotheses is correct, it is f_c is determined. Otherwise, ε plays a role of a tolerance for uncertainty in the measures or a confidence bound in the estimation under perturbed data.

Since there are no way to established f_c a priori other than to test for consistency for both, $f_c = 1$ and $f_c = 0$, then one must calculate (59) in both cases as explained in the next.

4.2. Using the algorithm

The estimation algorithm is finally established as described in the following. Starting with an initial vector $\left[\hat{\boldsymbol{\theta}}_x^{(0)\mathrm{T}}, \hat{\boldsymbol{\theta}}_z^{(0)\mathrm{T}}\right]^{\mathrm{T}}$ one iterates (59) for $f_c = 1$ and $f_c = 0$ independently. The estimation will be finished when in one of the cases it results in $\left|\hat{\theta}_{x_3}^{(m)} - \hat{\theta}_{z_3}^{(m)}\right| < \varepsilon$, for some specified small tolerance $\varepsilon > 0$, with $\hat{\theta}_{x_3}^{(m)} = \hat{a}_4 = 1/\hat{m}_{0_x} g$ and $\hat{\theta}_{z_3}^{(m)} = \hat{b}_4 = 1/\hat{m}_{0_z} g$. That one successful case will provide the parameters.

4.3. Convergence

The convergence of the algorithm is proved for monochromatic excitation in the following theorem.

Theorem 1. *(Convergence of the estimates) If the cable is excited by* $x(t) = A_x \sin(\omega_0 t)$ *and* $z(t) = A_z \sin(\omega_0 t + \varphi)$ *in the static configuration, the asymptotic convergence of* $\hat{\boldsymbol{\theta}}_x^{(m)}$ *and* $\hat{\boldsymbol{\theta}}_x^{(m)}$ *generated by (59) to the true values is guaranteed provided that*

1. for $f_c = 0$ (i.e. in Case II): $\left[\hat{a}_1^{(0)}, \hat{a}_3^{(0)}, \hat{a}_4^{(0)}\right]^{\mathrm{T}}, \left[\hat{b}_1^{(0)}, \hat{b}_3^{(0)}, \hat{b}_4^{(0)}\right]^{\mathrm{T}} \in \Re^3$
2. for $f_c = \mathbf{1}$ (i.e. in Case I): generated parameters $\hat{\boldsymbol{\theta}}_x^{(m)}$ and $\hat{\boldsymbol{\theta}}_z^{(m)}$ accomplish

$$\left\| \sum_{j=1}^{3} \frac{\partial \bar{k}_{3j}}{\partial \hat{a}_4} \mathbf{f}_{x_j} \right\| < 1 \tag{64}$$

$$\left\| \sum_{j=4}^{6} \frac{\partial \bar{k}_{6j}}{\partial \hat{b}_4} \mathbf{f}_{z_j} \right\| < 1 \tag{65}$$

for $m = 0, 1, 2, \ldots$, where $\bar{k}_{ij}$ are elements of $\mathbf{K}_t^{-1}$.

Proof. A sufficient condition for the parameter errors $\left(\hat{\boldsymbol{\theta}}_x^{(m)} - \hat{\boldsymbol{\theta}}_x^{(m-1)}\right)$ and $\left(\hat{\boldsymbol{\theta}}_z^{(m)} - \hat{\boldsymbol{\theta}}_z^{(m-1)}\right)$ generated by (59) to asymptotically converge to zero is that the continuous functions defined in (57) and (58) satisfy in some neighborhood of $\boldsymbol{\theta}_x$ and $\boldsymbol{\theta}_z$ (Bronstein and Semendjayew, 1987)

$$\left\|\frac{\partial \mathbf{g}_x^{\mathrm{T}}}{\partial \hat{\boldsymbol{\theta}}_x}\right\| > \left\|\frac{\partial \mathbf{h}_x^{\mathrm{T}}}{\partial \hat{\boldsymbol{\theta}}_x}\right\| \text{ and } \left\|\frac{\partial \mathbf{g}_z^{\mathrm{T}}}{\partial \hat{\boldsymbol{\theta}}_z}\right\| > \left\|\frac{\partial \mathbf{h}_z^{\mathrm{T}}}{\partial \hat{\boldsymbol{\theta}}_z}\right\|, \tag{66}$$

where $\|.\|$ is some induced matrix norm. As $\mathbf{g}_x =^{def} \hat{\boldsymbol{\theta}}_x$ and $\mathbf{g}_z =^{def} \hat{\boldsymbol{\theta}}_z$, thus

$$\left\|\frac{\partial \mathbf{h}_x^{\mathrm{T}}}{\partial \hat{\boldsymbol{\theta}}_x}\right\| < 1 \text{ and } \left\|\frac{\partial \mathbf{h}_z^{\mathrm{T}}}{\partial \hat{\boldsymbol{\theta}}_z}\right\| < 1. \tag{67}$$

Bearing (67) in mind, let us prove part (a). A glance at (61), for $f_c = 1$, reveals that the Jacobians $\left(\partial \mathbf{f}_x^{\mathrm{T}}/\partial \hat{\boldsymbol{\theta}}_x\right)\left(\hat{\boldsymbol{\theta}}_x\right)$ and $\left(\partial \mathbf{f}_z^{\mathrm{T}}/\partial \hat{\boldsymbol{\theta}}_z\right)\left(\hat{\boldsymbol{\theta}}_z\right)$ are not parametric, i.e. they depend exclusively on data H_j and V_j. Hence, the roots of $\mathbf{f}_x$ and $\mathbf{f}_z$ at $\hat{\boldsymbol{\theta}}_x = \boldsymbol{\theta}_x$ and $\hat{\boldsymbol{\theta}}_z = \boldsymbol{\theta}_z$ are simple, respectively. Taking the derivative of (58) it holds

$$\left[\frac{\partial \mathbf{h}_x^{\mathrm{T}}}{\partial \hat{\boldsymbol{\theta}}_x}\frac{\partial \mathbf{h}_z^{\mathrm{T}}}{\partial \hat{\boldsymbol{\theta}}_z}\right] = I - \mathbf{K}_t\mathbf{K}_t^{-1} - \begin{bmatrix} \partial \mathbf{A}_x & 0 \\ 0 & \partial \mathbf{A}_z \end{bmatrix}\mathbf{K}_t^{-1}\begin{bmatrix} \mathbf{f}_x \\ \mathbf{f}_z \end{bmatrix} = 0, \tag{68}$$

where

$$\partial \mathbf{A}_x = \left[\left[\frac{\partial}{\partial \hat{\boldsymbol{\theta}}_x}\right], \left[\frac{\partial}{\partial \hat{\boldsymbol{\theta}}_x}\right], \left[\frac{\partial}{\partial \hat{\boldsymbol{\theta}}_x}\right]\right] \tag{69}$$

$$\partial \mathbf{A}_z = \left[\left[\frac{\partial}{\partial \hat{\boldsymbol{\theta}}_z}\right], \left[\frac{\partial}{\partial \hat{\boldsymbol{\theta}}_z}\right], \left[\frac{\partial}{\partial \hat{\boldsymbol{\theta}}_z}\right]\right], \tag{70}$$

$$\left[\frac{\partial}{\partial \hat{\boldsymbol{\theta}}_x}\right]^{\mathrm{T}} = \left[\frac{\partial}{\partial \hat{\boldsymbol{\theta}}_{x_1}}, \frac{\partial}{\partial \hat{\boldsymbol{\theta}}_{x_2}}, \frac{\partial}{\partial \hat{\boldsymbol{\theta}}_{x_3}}\right]$$

and

$$\left[\frac{\partial}{\partial \hat{\boldsymbol{\theta}}_z}\right]^{\mathrm{T}} = \left[\frac{\partial}{\partial \hat{\boldsymbol{\theta}}_{z_1}}, \frac{\partial}{\partial \hat{\boldsymbol{\theta}}_{z_2}}, \frac{\partial}{\partial \hat{\boldsymbol{\theta}}_{z_3}}\right].$$

Consequently, the only condition for $\left\|\partial \mathbf{h}_x^{\mathrm{T}}/\partial \hat{\boldsymbol{\theta}}_x\right\| = \left\|\partial \mathbf{h}_z^{\mathrm{T}}/\partial \hat{\boldsymbol{\theta}}_z\right\| = 0$ is that for all t, $\partial \mathbf{f}_x^{\mathrm{T}}/\partial \hat{\boldsymbol{\theta}}_x$ and $\partial \mathbf{f}_z^{\mathrm{T}}/\partial \hat{\boldsymbol{\theta}}_z$ be uniformly regular in time with this condition fulfilled, the convergence for $f_c = 0$ is ensured. This is proved in the next.

The columns $\partial f_{x_j}/\partial \hat{a}_i$ for $j = 1, 2, 3$, are generated by the functional basis (see (61))

$$\xi_{f_c=0} = \left\{1,\ H(t)V(t),\ H(t)\sinh^{-1}\left(\frac{V(t)}{H(t)}\right) - V(t)\right\}. \tag{71}$$

In order for $\partial \mathbf{f}_x^{\mathrm{T}}/\partial \hat{\boldsymbol{\theta}}_x$ to be regular, its columns $\left[1,\ H_j V_j,\ \ H_j\ \sinh^{-1}(V_j/H_j) - V_j\right]^{\mathrm{T}}$ must be linear independent. This is achieved if the data pairs $\left(H_j, V_j\right)$ do not satisfy for all j the three conditions: $V_j = c/H_j$, $V_j = H_j\ \sinh((c + V_j)/H_j)$ and $V_j = H_j \sinh((cV_jH_j + V_j)/H_j)$, with c an arbitrary constant in each case. Now we analyze if $x(t) = A_x\ \sin(\omega_0 t)$ and $z(t) = A_z\ \sin(\omega_0 t + \varphi)$ generate function pairs $(H(t), V(t))$, which do not satisfy the above conditions.

From (49) and (50), for $f_c = 0$, and the condition $V(t) = c/(H(t))$ it holds

$$\sin(\omega_0 t) = c_0 + \frac{c_1}{H_x(t)} + c_2 H_x(t) \sinh^{-1}\left(\frac{c_3}{H_x^2(t)}\right) \tag{72}$$

$$\sin(\omega_0 t + \varphi) = c_4 + \frac{c_5}{H_z^2(t)} + c_6 H_z(t)\left(\sqrt{1 + \frac{c_7}{H_z^4(t)}} - 1\right) \tag{73}$$

with c_i real constants and $H_x : \Re^+ \to \Re$ and $H_z : \Re^+ \to \Re$ time assignments. If there would exist some assignment $H_x(t)$ and $H_z(t)$ that satisfy (72) and (73) simultaneously for all t, respectively, then it would be valid $H_z(t) = H_x(t + (\varphi/\omega_0))$. But this is contradictory because both right sides at (72) and (73) are analytically different. Then the monochromatic signals $x(t)$ and $z(t)$ do not generate pairs $(H(t), c/H(t))$. The same argumentation can be easily extended to $(H(t), H(t)\ \sinh((c + V(t))/(H(t))))$ and $(H(t), H(t)\ \sinh((cV(t)H(t) + V(t))/(H(t))))$, and conclude that these pairs cannot be generated by such signals. So, the columns $\left[1, H_j V_j, H_j\ \sinh^{-1}(V_j/H_j) - V_j\right]^{\mathrm{T}}$ of $\partial \mathbf{f}_x^{\mathrm{T}}/\partial \hat{\boldsymbol{\theta}}_x$ result linear independent for harmonic signals $x(t)$ and $z(t)$.

Analogously, it can be proved the uniform regularity for $\partial \mathbf{f}_z^{\mathrm{T}}/\partial \hat{\boldsymbol{\theta}}_z$ using the same arguments to generate the columns $\partial f_{z_j}/\partial \hat{b}_i$ for $j = 1, 2, 3$ by the functional basis (see (61))

$$\zeta_{f_c=0} = \left\{1, V^2(t), H(t)\left(\sqrt{1 + \left(\frac{V(t)}{H(t)}\right)^2} - 1\right)\right\}. \tag{74}$$

Therefore, the convergence of the parameter errors $\left(\hat{\boldsymbol{\theta}}_x^{(m)} - \hat{\boldsymbol{\theta}}_x^{(m-1)}\right)$ and $\left(\hat{\boldsymbol{\theta}}_z^{(m)} - \hat{\boldsymbol{\theta}}_z^{(m-1)}\right)$ asymptotically to zero is ensured for any initial conditions $\left[\hat{a}_1^{(0)}, \hat{a}_3^{(0)}, \hat{a}_4^{(0)}\right]^{\mathrm{T}}, \left[\hat{b}_1^{(0)}, \hat{b}_3^{(0)}, \hat{b}_4^{(0)}\right]^{\mathrm{T}} \in \Re^3$.

Part (b) of the Theorem 1 involves the case $f_c = 1$. As the Jacobians $\left(\partial \mathbf{f}_x^{\mathrm{T}}/\partial \hat{\boldsymbol{\theta}}_x\right) \times \left(\hat{\boldsymbol{\theta}}_x\right)$ and $\left(\partial \mathbf{f}_z^{\mathrm{T}}/\partial \hat{\boldsymbol{\theta}}_z\right)\left(\hat{\boldsymbol{\theta}}_z\right)$ are parametric, they depend not only on data but also

on parameters. Hence, the roots of $\mathbf{f}_x$ and $\mathbf{f}_z$ at $\hat{\boldsymbol{\theta}}_x = \boldsymbol{\theta}_x$ and $\hat{\boldsymbol{\theta}}_z = \boldsymbol{\theta}_z$ are both not simple. Taking the derivative of (58) for $f_c = 1$ and considering (67), it holds

$$\left\| \frac{\partial \mathbf{h}_x^{\mathrm{T}}}{\partial \hat{\boldsymbol{\theta}}_x} \right\| = \left\| \partial \mathbf{A}_x \left[\frac{\partial \mathbf{f}_x^{\mathrm{T}}}{\partial \hat{\boldsymbol{\theta}}_x} \right]^{-1} \mathbf{f}_x \right\| < 1 \tag{75}$$

$$\left\| \frac{\partial \mathbf{h}_z^{\mathrm{T}}}{\partial \hat{\boldsymbol{\theta}}_z} \right\| = \left\| \partial \mathbf{A}_z \left[\frac{\partial \mathbf{f}_z^{\mathrm{T}}}{\partial \hat{\boldsymbol{\theta}}_z} \right]^{-1} \mathbf{f}_z \right\| < 1. \tag{76}$$

From the above it is concluded that the Jacobians $\partial \mathbf{f}_x^{\mathrm{T}}/\partial \hat{\boldsymbol{\theta}}_x$ and $\partial \mathbf{f}_z^{\mathrm{T}}/\partial \hat{\boldsymbol{\theta}}_z$ must be regular for the given harmonic signals. To evidence this property we note that the columns $\partial f_{x_j}/\partial \hat{a}_i$, for $j = 1, 2, 3$, are created by the functional basis (see (61))

$$\xi_{f_c=1} = \left\{ 1, H(t), \frac{-L_0}{\hat{a}_4 \sqrt{1 + \left(\dfrac{V(t) - L_0/\hat{a}_4}{H(t)} \right)^2}} + H(t) \left(\sinh^{-1}\left(\frac{V(t)}{H(t)} \right) - \sinh^{-1}\left(\frac{V(t) - L_0/\hat{a}_4}{H(t)} \right) \right) \right\}.$$

The columns

$$\left[1, H_j, \frac{-L_0}{\hat{a}_4 \sqrt{1 + \left(\dfrac{V_j - L_0/\hat{a}_4}{H_j} \right)^2}} + H_j \left(\sinh^{-1}\left(\frac{V_j}{H_j} \right) - \sinh^{-1}\left(\frac{V_j - L_0/\hat{a}_4}{H_j} \right) \right) \right]^{\mathrm{T}}$$

are linear independent if (H_j, V_j) do not satisfy for all j the condition $F_n = cF_m$ with $n, m = 1, 2, 3, n \neq m$, F_n and F_m being two different functions of the basis (77).

Again, using the same argumentation, we can ascertain that the harmonic signals $x(t)$ and $z(t)$ generate function pairs $(H(t), V(t))$, which do not satisfy the above conditions. So, linear independent columns of $\partial \mathbf{f}_x^{\mathrm{T}}/\partial \hat{\boldsymbol{\theta}}_x$ are generated.

The extension of these results to $\partial \mathbf{f}_z^{\mathrm{T}}/\partial \hat{\boldsymbol{\theta}}_z$ technically similar as done for $\partial \mathbf{f}_x^{\mathrm{T}}/\partial \hat{\boldsymbol{\theta}}_x$. The function basis for generation of the columns $\partial f_{z_j}/\partial \hat{b}_i$, for $j = 1, 2, 3$, is

(see (61))

$$\zeta_{f_c=1} = \left\{ 1, V(t), \frac{-L_0\left(V(t) - L_0/\hat{b}_4\right)}{\hat{b}_4 H\sqrt{1+\left(\dfrac{V(t)-L_0/\hat{b}_4}{H(t)}\right)^2}} + H(t)\left(\sqrt{1+\left(\frac{V(t)}{H(t)}\right)^2} - \sqrt{1+\left(\frac{V(t)-L_0/\hat{b}_4}{H(t)}\right)^2}\right)\right\}. \tag{78}$$

It is direct to deduce conditions for H_j and V_j that are not satisfied by the generated signals $H(t)$ and $V(t)$ through the harmonic excitation. In this way, linear independent columns of $\partial \mathbf{f}_z^{\mathrm{T}}/\partial \hat{\boldsymbol{\theta}}_z$ are created. Consequently $\mathbf{K}_t$ is also uniform regular in time for $f_c = 1$.

Finally, it is straightforward to see that conditions (75) and (76) can be transformed into (64) and (65). Thus for every $\hat{\boldsymbol{\theta}}_x^{(m)}$ and $\hat{\boldsymbol{\theta}}_z^{(m)}$ generated by the algorithm, from $m = 0$ in advanced, (64) and (65) must be satisfied in order to guarantee convergence. This concludes the proof of Theorem 1.

4.4. Estimation in the quasi-static dynamics

In comparison with the static behavior, the dynamic one introduces superharmonics in the frequency response of the forces. These components are the more intense the larger is the velocity of the upper end of the cable. The extension of the proposed method for these responses is feasible when the motions are slow. We assume furthermore that the moored structure has a large inertia so that it imposes low-frequency motions to the cables.

From the construction of manifolds in time it is inferred that the algorithm is sensible to the first and second derivatives of the forces. The reason reclines in the fact that if the sample points t_1, t_2, t_3 are taken sufficiently close each other, every mismatch between the dynamic force with respect to the static one will influence the estimates. This effect can be reduced by taking a smaller number of significative parameters and by using filtering of on-line estimates.

In control of moored structures it is important to know the mass density m_0 and the depth h_0. Additionally, this last one may vary slowly in time changing the force–position characteristics significantly. Other parameters like the lengths L_0 and l_0 are usually known in the set-up of the configuration of the catenaries. From this point of view, a smaller parameter set like $\{h_0, m_0\}$ will be less sensible to the derivatives of the forces.

A crucial point in the evaluation of the estimates is the definition of a "*success–fail*"-function, which determines how large is the confidence of the estimates. Such

a function may be implemented in the same manner as the function f_c. Thus, for some confidence bound ε

$$\sigma(t) = \begin{cases} 1 & \text{if } \left|\hat{a}_4 - \hat{b}_4\right| \leq \varepsilon \\ 0 & \text{if } \left|\hat{a}_4 - \hat{b}_4\right| > \varepsilon \end{cases} \tag{79}$$

describes a binary function, which evaluates the accuracy of the estimates. So, only estimates for $\sigma(t) = 1$ are considered.

The time evolution of the estimation under perturbed data can be nonsmooth, mainly for high-frequency excitation. As usually the excitation has zero mean, the estimation errors will fluctuate with the fundamental period of the motion. In order to capture the mean value of the estimate trajectories, a low-pass filtering is recommended. For this purpose $\bar{\boldsymbol{\theta}}_x(t)$ and $\bar{\boldsymbol{\theta}}_z(t)$ from

$$\tau\dot{\bar{\boldsymbol{\theta}}}_x(t) = -\bar{\boldsymbol{\theta}}_x(t) + \hat{\boldsymbol{\theta}}_x(t) \tag{80}$$

$$\tau\dot{\bar{\boldsymbol{\theta}}}_z(t) = -\bar{\boldsymbol{\theta}}_z(t) + \hat{\boldsymbol{\theta}}_z(t), \tag{81}$$

are taken as the estimates instead of $\hat{\boldsymbol{\theta}}_x(t)$ and $\hat{\boldsymbol{\theta}}_z(t)$. The filter time constant τ is defined according to the fundamental frequency of the excitation.

5. Simulations

The simulations are prepared on the basis of the dynamic and static configuration described in Section 2. The proposed algorithm runs on-line with a fixed parameter uncertainty bound $\varepsilon = 0.01$ and $\tau = 40$ [s] for all experiments. Let us consider a cable with coefficients $L_0 = 287.79$ [m], $l_0 = 250$ [m], $h_0 = 100$ [m], $m_0 = 22.3$ [kg], $EA_0 = 10^{10}$ [N].

5.1. Case-study 1: monochromatic excitation

We excite the upper end of the cable with

$$x(t) = 16\sin(\omega_0 t);\ z(t) = \frac{16}{3}\sin(\omega_0 t), \tag{82}$$

where the excitation frequency ω_0 will take different values. Let us now apply the algorithm on-line in the simulations as explained before.

First we consider the static configuration subject to Eqs. (14)–(16). The static forces V and H are depicted in Fig. 5 for $\omega_0 = 0.15$ [rad/s], whose evolutions show a typical sharp crest and flat valley. In Fig. 6, one sees the distortion suffered by the forces due to hydrodynamic drag effects. This distortion affects the symmetry (specially of the $V(t)$) as well as the intensity. Consequently, their Fourier transform functions embrace a wider frequency band as well as nonzero real and imaginary components.

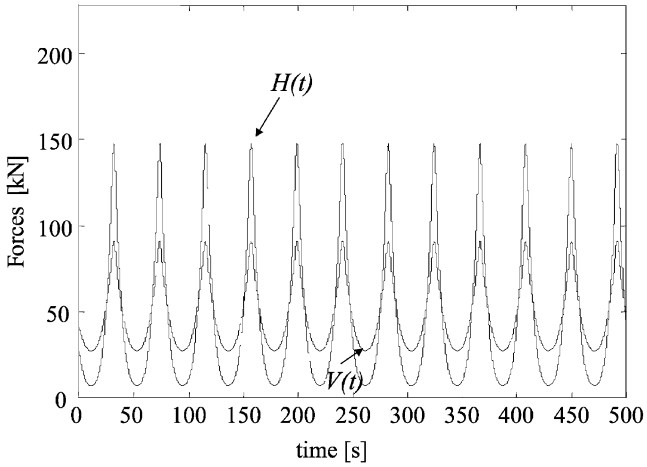

Fig. 5. Time evolution of static cable forces at the upper end for $\omega_0 = 0.15$ [rad/s].

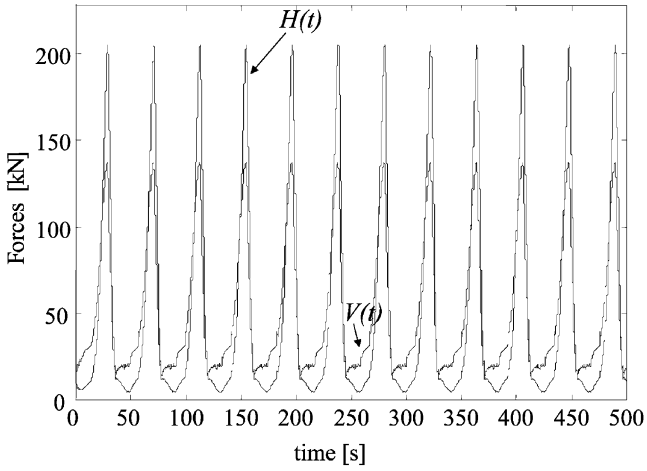

Fig. 6. Time evolution of dynamic cable forces at the upper end for $\omega_0 = 0.15$ [rad/s].

In the successive figures, the dynamic configuration is tested for $\omega_0 = 0.05$ and $\omega_0 = 0.15$ [rad/s], which are considered to lie in the range of the frequency response of floating structures.

Figs. 7 and 9 show the estimation of the mass density in the test frequencies, and Figs. 8 and 10 portray the corresponding evolutions of the estimated depth, respectively. Clearly, the lower is the excitation frequency the more precise is the estimation. Nevertheless, the estimations for the highest frequency $\omega_0 = 0.15$ [rad/s] are sufficiently exact for control purposes, having a mean error under 5% with respect to the true values.

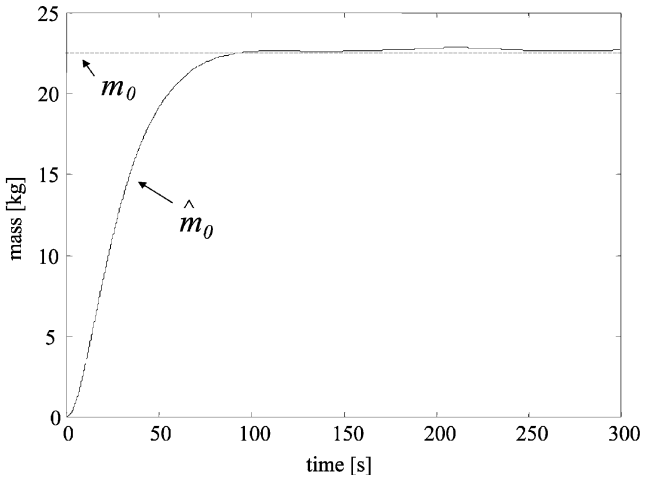

Fig. 7. Time evolution of the estimated cable mass density for $\omega_0 = 0.05$ [rad/s].

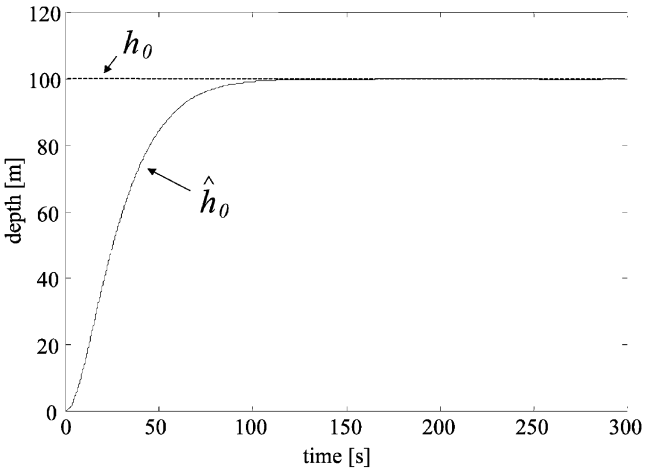

Fig. 8. Time evolution of the estimated depth for $\omega_0 = 0.05$ [rad/s].

5.2. Case-study 2: dominant resonance frequency

This case study pretends to depict the mooring line dynamics subject to a typical motion of semisubmersibles having a slight-damped and slow movement in the surge direction with a resonance frequency of $\omega_r = 0.012$ [rad/s] and an induced displacement due to a wave with $\omega_0 = 0.43$ [rad/s].

The evolution of the forces and estimates is reproduced in the Figs. 11, 13 and 14. Fig. 12 shows the progress of the function f_c. It has a stable course at one and

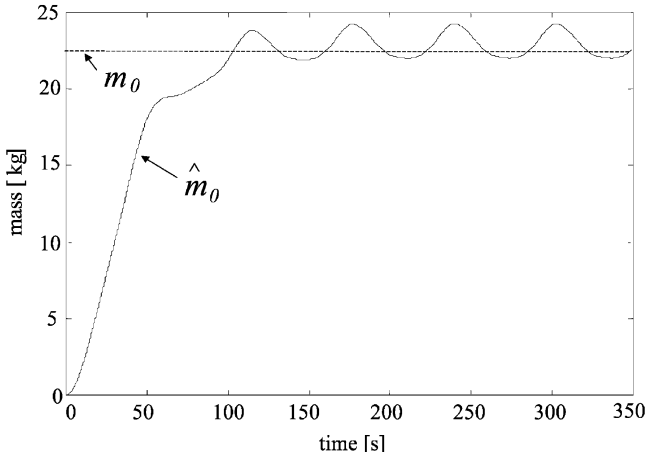

Fig. 9. Time evolution of the estimated cable mass density for $\omega_0 = 0.15$ [rad/s].

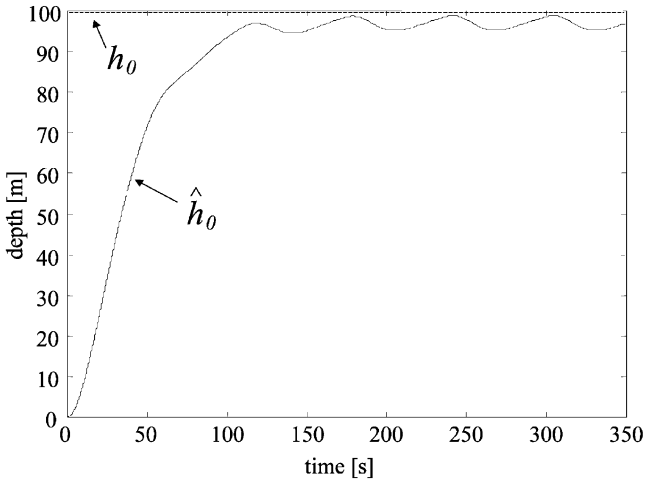

Fig. 10. Time evolution of the estimated depth for $\omega_0 = 0.15$ [rad/s].

zero values, except for short periods accounting for the case transition due to the uncertainty in the data.

It is remarkable that the high-frequency motion induced by a wave, influences the forces much more significantly for the case $f_c = 1$ (i.e. $\phi_s > 0$) than for the case $f_c = 0$ (i.e. $\phi_s = 0$).

Even when the high frequency of the wave produces a great distortion of the forces with respect to the static case, the estimates develop with high accuracy mainly far away from transition periods of f_c.

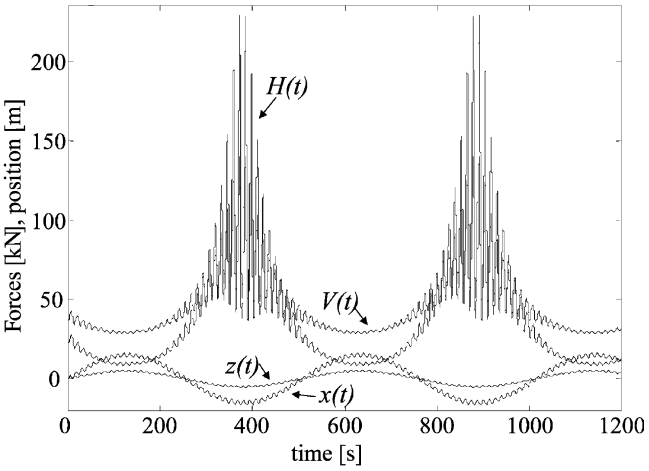

Fig. 11. Time evolution of dynamic cable forces and upper end position for the case-study 2.

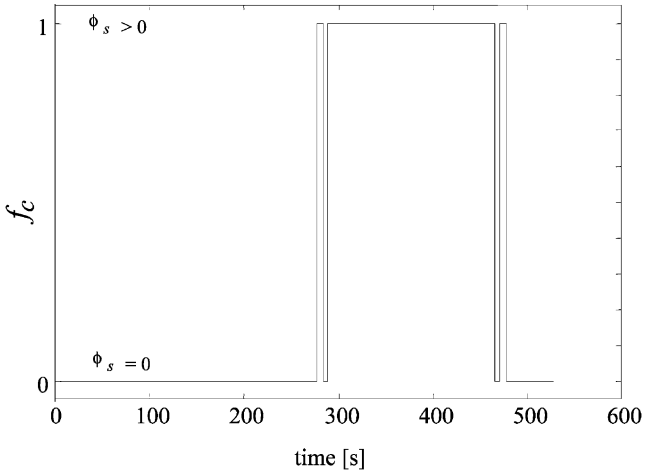

Fig. 12. Time evolution of the case-sensitive function f_c.

5.3. Case-study 3: time-varying depth

This case concerns the ability of the algorithm to adaptively tracking of parameter variations. To simulate the depth variation of h_0 we choose a law according to

$$h_0(t) = h_0 + 10\sin(0.001t), \tag{83}$$

where the mean value h_0 remains at the former value 100 [m]. The coordinates $x(t)$ and $z(t)$ behave also harmonic with $\omega_0 = 0.1$ [rad/s]. The evolution of forces is depicted in Fig. 15, which shows a variation of their amplitudes of about 50%

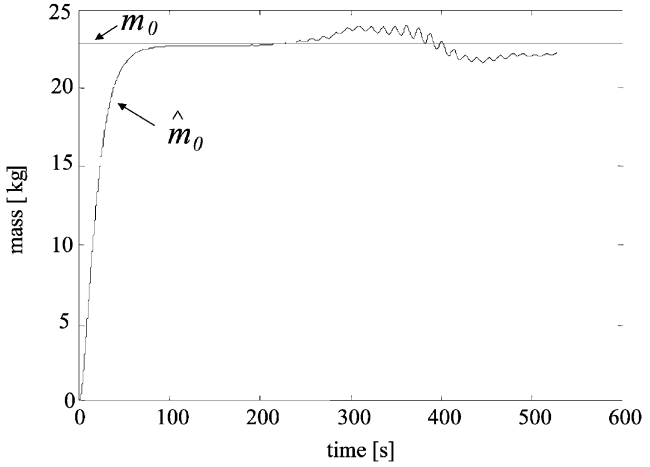

Fig. 13. Time evolution of the estimated cable mass density for case-study 2.

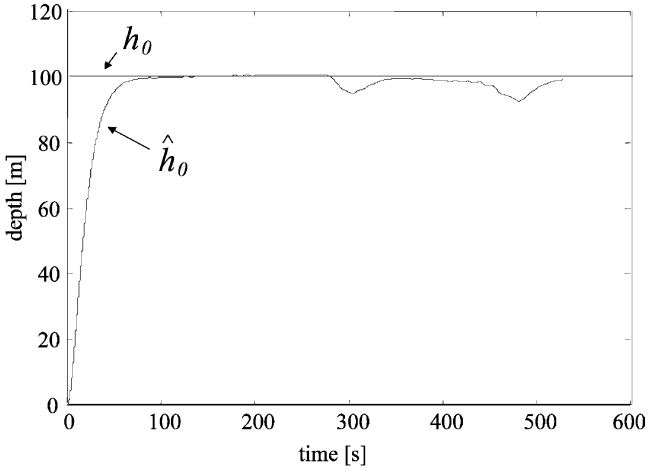

Fig. 14. Time evolution of the estimated depth for case-study 2.

against 10% of change in the depth. The mass density m_0 is estimated with high accuracy as shown in Fig. 16. Fig. 17 exemplifies the tracking of the time-varying depth. The maximal error for this estimation was below 3% with respect to the true value of the parameter.

6. Conclusions

In this paper, an adaptive algorithm for on-line estimation of physical coefficients of cables in viscous environment is presented. The procedure is useful for

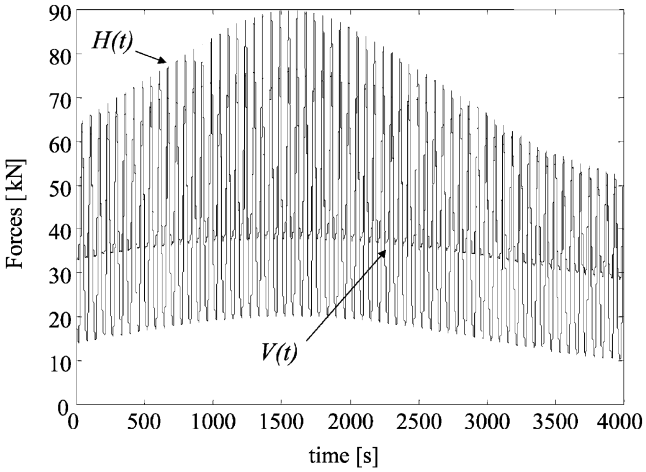

Fig. 15. Time evolution of dynamic cable forces for the case-study 3.

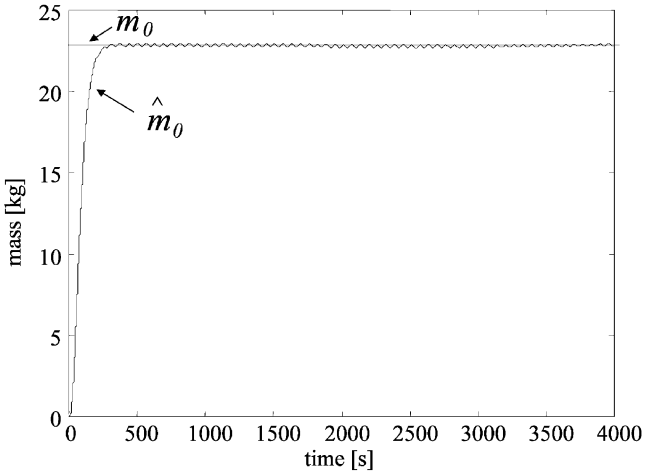

Fig. 16. Time evolution of the estimated cable mass for case-study 3.

obtaining cable characteristics, which are needed in stability analysis and control system design for moored floating structures. It uses measurements of position and forces, which usually are available from on-board instrumentation. The algorithm is also able to track changes in the depth. It is based on nonlinear solvers, which can cope with transcendental functions that are present in the model structure of the static configuration. Additionally it tests consistency of parameters in order to confer the estimation robustness with respect to dynamic perturbations in the data.

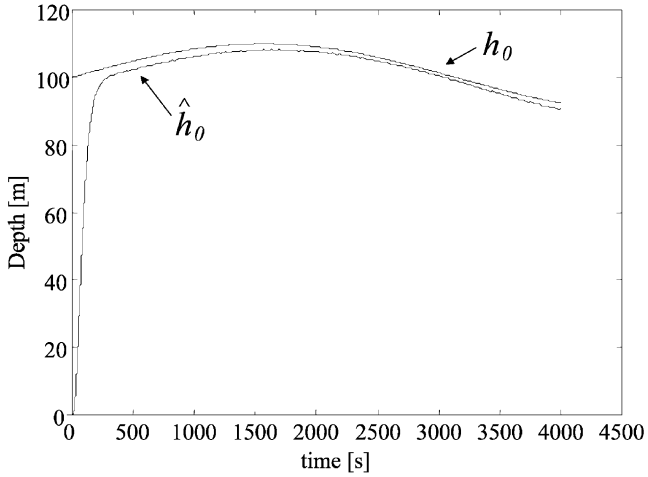

Fig. 17. Time evolution of the estimated time-varying depth for case-study 3.

The proof of asymptotic convergence of the estimates in the static configuration is an important part of the paper.

The influences of drag forces and hydrodynamic high-frequency effects in the estimation are taken into account as perturbations and constitute, consequently, the uncertainty of the system. These effects are tested by simulations. There were analyzed three basic case studies, concerning a monochromatic excitation, dominant resonance motion together with high-frequency waves, and finally slow time-varying depth. The results show that physical coefficients like depth and cable mass density can be estimated at the worst case with a mean error smaller than 5% of the exact value.

The proposed algorithm of this paper can be straightforwardly be extended to systems of catenaries with different parameters attached to a moored floating structure.

Acknowledgements

The authors thank Prof. Dr.-Ing. Edwin Kreuzer and Dr.-Ing. Volker Schlegel at the Technical University of Hamburg–Harburg for the theoretical support and test facilities. We are also grateful to Dipl-Ing. Ulrich Wilke for supplying simulation tools in the dynamic configuration. Dr. Mario Jordán, thanks also CONICET and Scientific Cooperation Project with Germany (AL/A99 - EX II/17) for financial supporting of this investigation.

References

Aamo, O.M., Fossen, T.I., 1999. Controlling line tension in thruster assisted mooring systems. IEEE International Conference on Control Applications, Hawaii.

Beltrán-Aguedo, R., Redín, F., García, A., Jordán, M.A., 2002. A study of persistency of excitation for semisubmersible systems with chaotic behaviour. 15th Triennial IFAC World Congress, Barcelona.

Beltrán-Aguedo, R., Jordán, M.A., 2003. A method for continuous-time identification of moored systems. Latin American Applied Research 33 (4), 483–488.

Bhattacharyya, S.K., Selvam, R.P., 2001. Parameter identification of a large moored floating body in random ocean waves by reverse miso method. 20th Offshore Mechanics and Artic Engineering Conference, Rio de Janeiro.

Bronstein, I.N., Semendjayew, K.A., 1987. Tashenbuch der Mathematik. Verlag Harri Deutsch, Thun.

Chatjigeorgiou, I.K., Mavrakos, S.A., 2000. Comparative evaluation of numerical schemes for 2d mooring dynamics. International Journal of Offshore and Polar Engineering 10, 301–309.

Dmitrieva, I., Lougovsky, V., 1997. Non-linear harmonic, subharmonic and chaotic motion of offshore structures. In: Eighth International Conference on the Behaviour of Offshore Structures, Delft.

Gottlieb, O., Feldman, M., Yim, S.C.S., 1996. Parameter identification of nonlinear ocean mooring systems using the Hilbert transform. Journal of Offshore Mechanics and Arctic Engineering 118, 29–36.

Gottlieb, O., Yim, S.C.S., 1997. Nonlinear dynamics of a coupled surge-heave small-body ocean mooring system. Ocean Engineering 24 (5), 479–495.

Irvine, M., 1992. Cable Structures. Dover Publications, Inc, New York.

Kreuzer, E., Ellermann, K., Markiewicz, M., 2002. Nonlinear dynamics of floating cranes. Nonlinear Dynamics 27, 107–183.

Mavrakos, S.A., Papazoglou, V.J., Triantafyllou, M.S., Chatjigeorgiou, I.K., 1996. Deep water mooring dynamics. Marine Structures 9, 181–209.

Mavrakos, S.A., Chatjigeorgiou, I.K., 1997. Dynamic behaviour of deep water mooring lines with submerged buoys. Computers and Structures 64, 819–835.

Papazoglou, V.J., Mavrakos, S.A., Triantafyllou, M.S., 1996. Non-linear cable response and model testing in water. Journal of Sound and Vibration 140, 103–115.

Selvam, R.P., Bhattacharyya, S.K., 2001. Parameter identification of a compliant non-linear sdof system in random ocean waves by reverse miso method. Ocean Engineering 28 (9), 1199–1223.

Sorensen, A., Strand, J.P., Fossen, T.I., 1999. Thruster assisted position mooring system for turret-anchored fpsos. In: IEEE International Conference on Control Applications, Hawaii.